J Therm Anal Calorim (2015) 121:1151–1157
DOI 10.1007/s10973-015-4906-4

Phase relationships of the *R*–Al–Si systems

The Pr–Al–Si isothermal section at 500 °C

Anna Maria Cardinale[1] · Daniele Macciò[1] · Adriana Saccone[1]

Received: 22 December 2014 / Accepted: 25 June 2015 / Published online: 23 July 2015

Abstract In the framework of a systematic investigation of intermetallic systems, constituted by aluminium and silicon with a rare earth metal, the isothermal section at 500 °C of the Pr–Al–Si system has been experimentally investigated. The experimental techniques used were scanning electron microscopy, electron microprobe analysis and X-ray powder diffraction, and some samples have been analysed by differential thermal analysis. The existence of six ternary compounds has been confirmed, one of them showing a composition homogeneity range: τ_1 $PrAl_2Si_2$ (hP5-Ce_2SO_2 type), τ_2 $Pr_3Al_4Si_6$ (hP13-$Ce_3Al_4Si_6$ type), τ_3 $PrAlSi_2$ (hP8-$CeAlSi_2$ type), τ_4 Pr_2Al_3Si (hP3-AlB_2 type), τ_5 $PrAl_{(1-x)}Si_{(1+x)}$ (tI12-αThSi$_2$Si type) and τ_6 Pr_2AlSi (oS8-CrB type). A few compounds pertaining to the binary boundary systems Pr–Al and Pr–Si dissolve the third element.

Keywords Phase diagrams · Intermetallic compounds · Aluminium alloys · Rare earth alloys · Silicon alloys

Introduction

Multicomponent Al–Si-based alloys are important and widely used in industries; the addition of a rare earth metal to Al–Si alloys can result in an increase in their extremely useful thermal, mechanical and corrosion resistance properties; this implies the need for the development in alloys' composition design. The addition of a rare earth element (*R*) can improve the technological properties and the stability at high temperatures of these alloys, through the formation of ternary phases [1–5]. Moreover, the addition of rare earth metals to casting Al–Si alloys modifies their microstructures [6] inducing a lowering of the eutectic temperature; for this reason, a measure of the "depression" in the eutectic temperature value has been proposed as a method to control the modification level in the alloy microstructure by means of thermal analysis measurements [7, 8].

To improve the understanding of the rare earths' influence on the Al–Si alloy properties, the knowledge of the phase relationships and the constitutional properties of the ternary *R*–Al–Si systems can constitute an important support. For this purpose, the investigation of the different *R*–Al–Si systems (*R* = rare earth) is part of an ongoing research project by our research group with the aim to clarify the constitutional properties of these ternary systems ([9–11] and references therein). In this work, the Pr–Al–Si isothermal section at 500 °C, in the full concentration range, has been experimentally investigated by using scanning electron microscopy (SEM), electron microprobe analysis (EDXS), X-ray powder diffraction (XRPD) and differential thermal analysis (DTA). Some samples have been analysed by DTA.

Literature data

Boundary binary systems

The Al–Si phase diagram, based mainly on the work by Murray et al. [12], consists of a simple eutectic system with the eutectic reaction at 12.2 at.% Si and 577 °C. The Pr–Si

✉ Anna Maria Cardinale
cardinal@chimica.unige.it

[1] Dipartimento di Chimica e Chimica Industriale, Università di Genova, Via Dodecaneso, 31, 16146 Genoa, Italy

Table 1 SEM–EDX and XRPD data on the Pr–Al–Si samples annealed at 500 °C

N	Nominal composition Pr, Al, Si/at.%	Phases crystal structure	EDXS results Pr, Al, Si/at.%	Lattice parameters/nm		
				a	*b*	*c*
1	8.5, 36.5, 55.0	Si *cF8-*C_{diam}	0.0, 0.0, 100.0	0.5428 (1)		
		Al *cF4-Cu*	1.0, 97.0, 2.0	0.4044 (1)		
		τ_1 *hP5-*$CaAl_2Si_2$	22.0, 38.0, 40.0	0.4208 (1)		0.6826 (7)
2	14.0, 20.0, 66.0	Si *cF8-*C_{diam}	0.0, 0.0, 100.0	0.5422 (2)		
		τ_1 *hP5-*$CaAl_2Si_2$	20.5, 37.0, 42.0	0.4203 (3)		0.6813 (7)
		τ_2 *hP13-*$Ce_3Al_4Si_6$	23.0, 30.5, 46.5	0.4189 (6)		1.7868 (6)
3	15.0, 14.5, 70.5	Si *cF8-*C_{diam}	0.0, 0.0, 100.0	0.5427 (2)		
		τ_2 *hP13-*$Ce_3Al_4Si_6$	25.0, 30.0, 45.0	0.4172 (2)		1.7936 (9)
		τ_3 *hP8-*$CeAlSi_2$	27.0, 25.5, 47.5	0.4161 (2)		1.1105 (8)
4	21.5, 53.5, 25.0	Al *cF4-Cu*	3.5, 94.0, 2.0	0.4045 (2)		
		τ_1 *hP5-*$CaAl_2Si_2$	19.0, 44.5, 36.5	0.4211 (2)		0.6800 (2)
		τ_5 *tI12-*$\alpha ThSi_2$	36.0, 26.0, 38.0	0.4219 (1)		1.3748 (9)
5	23.0, 25.0, 52.0	Si *cF8-*C_{diam}	0.0, 0.0, 100.0	0.5448 (6)		
		τ_2 *hP13-*$Ce_3Al_4Si_6$	24.0, 31.0, 45.0	0.4172 (2)		1.7996 (9)
		τ_3 *hP5-*$CaAl_2Si_2$	26.0, 26.0, 48.0	0.4157 (1)		1.1101 (8)
6	24.5, 62.0, 13.5	Al *cF4-Cu*	0.0, 98.0, 2.0	0.4041 (1)		
		τ_5 *tI12-*$\alpha ThSi_2$	35.5, 36.5, 28.0	0.4225 (1)		1.4533 (7)
		αPr_3 Al_{11} *oI28-*La_3Al_{11}	24.0, 75.5,0.5	0.4372 (2)	1.0022 (5)	1.2948 (8)
7	24.5, 73.0, 2.5	Pr Al_3 *hP8-*Ni_3Sn	27.0, 70.0, 3.0	0.6465 (5)		0.4588 (5)
		αPr_3 Al_{11} *oI28-*La_3Al_{11}	23.0, 76.0, 0.0	0.4373 (3)	1.0018 (6)	
		τ_5 *tI12-*$\alpha ThSi_2$	32.5, 36.5, 31.0	0.4210 (5)		1.3673 (9)
8	26.0, 12.5, 61.5	Si *cF8-*C_{diam}	1.0, 1.0, 98.0	0.5475 (8)		
		τ_3 *hP8-*$CeAlSi_2$	25.5, 25.0, 49.5	0.4158 (3)		1.1122 (3)
		$\beta Pr(Al_xSi_{1-x})_2$ *tI12-*$\alpha ThSi_2$	33.5, 15.0, 51.5	0.4218 (2)		1.3817 (2)
9	30.0, 11.0, 59.0	Si *cF8-*C_{diam}	0.0, 0.0, 100.0	0.5430 (2)		
		$\beta Pr(Al_xSi_{1-x})_2$ *tI12-*$\alpha ThSi_2$	35.0, 11.0, 54.0	0.4217 (2)		1.3798 (2)
10	26.5, 30.0, 43.5	τ_2 *hP13-*$Ce_3Al_4Si_6$	25.0, 31.0, 44.0	0.4176 (1)		1.7927 (1)
		τ_3 *hP8-*$CeAlSi_2$	27.0, 27.0, 46.0	0.4161 (4)		1.1182 (4)
		τ_5 *tI12-*$\alpha ThSi_2$	35.0, 27.5, 37.5	0.4215 (2)		1.4447 (9)
11	28.0, 24.5, 47.5	τ_2 *hP13-*$Ce_3Al_4Si_6$	26.0, 29.0, 45.0	0.4159 (3)		1.7999 (9)
		τ_3 *hP8-*$CeAlSi_2$	27.0, 26.0, 47.0	0.4155 (2)		1.1113 (8)
		τ_5 *tI12-*$\alpha ThSi_2$	36.5, 26.5, 37.0	0.4217 (3)		1.4421 (9)
12	28.0, 33.5, 38.5	Al *cF4-Cu*	89.0, 5.0, 6.0	0.4058 (9)		
		τ_1 *hP5-*$CaAl_2Si_2$	22.0, 37.0, 41.0	0.4200 (5)		0.6831 (5)
		τ_5 *tI12-*$\alpha ThSi_2$	36.0, 27.5, 36.5	0.4211 (1)		1.4424 (1)
13	32.5, 59.0, 7.5	$PrAl_2$ *cF24-*$MgCu_2$	37.5, 62.0, 1.0	0.8020 (1)		
		τ_4 hP3-AlB_2	37.0, 45.5, 17.5	0.4291 (2)		0.4248 (2)
		Pr Al_3 *hP8-*Ni_3Sn	28.5, 67.5, 4.0	0.6486 (5)		0.4594 (5)
14	34.5, 19.0, 46.5	$\beta Pr(Al_xSi_{1-x})_2$ *tI12-*$\alpha ThSi_2$	35.0, 12.0, 53.0	0.4225 (2)		1.3851 (9)
		τ_5 *tI12-*$\alpha ThSi_2$	35.0, 26.0, 39.0	0.4215 (3)		1.3701 (9)
15	41.0, 3.5, 55.5	$Pr(Al_xSi_{1-x})$ *oP8-FeB*	51.0, 0.0, 49.0	0.8822 (5)	0.3936 (2)	0.5914 (3)
		$\beta Pr(Al_xSi_{1-x})_2$ *tI12-*$\alpha ThSi_2$	36.5, 4.5, 59.0	0.4221 (3)		1.3773 (9)
16	40.5, 19.0, 40.5	$Pr(Al_xSi_{1-x})$ *oP8-FeB*	51.0, 2.0, 47.0	0.8228 (4)	0.3954 (2)	0.5914 (5)
		τ_5 *tI12-*$\alpha ThSi_2$	36.5, 25.5, 38.0	0.4211 (1)		1.4447 (9)
17	37.0, 34.0, 29.0	τ_5 *tI12-*$\alpha ThSi_2$	36.0,34.0, 30.0	0.4227 (1)		1.4450 (1)
19	40.0, 41.0, 19.0	τ_6 *oS8-CrB*	53.0, 25.0, 22.0	0.4463 (5)	1.1236 (9)	0.4022 (9)
		τ_4 hP3-AlB_2	36.5, 46.0, 17.5	0.4296 (3)		0.4256 (4)

Table 1 continued

N	Nominal composition Pr, Al, Si/at.%	Phases crystal structure	EDXS results Pr, Al, Si/at.%	Lattice parameters/nm		
				a	*b*	*c*
19	42.5, 32.5, 26.5	$Pr(Al_xSi_{1-x})$ *oP8-FeB*	51.0, 10.0, 39.0	0.8197 (2)	0.3938 (8)	0.5945 (5)
		τ_4 hP3-AlB_2	37.0, 41.0, 22.0	0.4301 (5)		0.4255 (7)
20	42.0, 24.0, 34.0	τ_5 *tI12-*$\alpha ThSi_2$	36.0, 35.0, 29.0	0.4229 (4)		1.4478 (3)
		$Pr(Al_xSi_{1-x})$ *oP8-FeB*	48.0, 10.5, 41.5	0.8222 (6)	0.3962 (2)	0.5929 (3)
21	44.5, 19.5, 36.0	$Pr(Al_xSi_{1-x})$ *oP8-FeB*	51.0, 0.0, 48.5	0.8238 (3)	0.3938 (1)	0.5925 (2)
		τ_5 *tI12-*$\alpha ThSi_2$	36.0, 35.0, 29.0	0.4227 (3)		1.4407 (2)
22	47.0, 47.5, 5.5	$PrAl_2$ *cF24-MgCu*	37.0, 63.0, 0.0	0.8020 (2)		
		$Pr(Al_xSi_{1-x})$ *oP8-FeB*	54.5, 43.0, 2.5	0.5955 (4)	1.1750 (9)	0.5729 (6)
		τ_6 *oS8-CrB*	60.0, 20.0, 20.0	0.4476 (5)	1.1273 (6)	0.4070 (3)
23	49.0, 19.0, 32.0	τ_4 hP3-AlB_2	37.5, 42.0, 20.5	0.4297 (9)		0.4254 (4)
		τ_6 *oS8-CrB*	49.5, 19.0, 31.5	0.4460 (5)	1.1238 (8)	0.4082 (3)
		$Pr(Al_xSi_{1-x})$ *oP8-FeB*	50.5, 8.5, 41.0	0.8227 (9)	0.3952 (9)	0.5923 (8)
24	52.5, 9.5, 38.0	$Pr(Al_xSi_{1-x})$ *oP8-FeB*	49.0, 8.0, 43.0	0.8250 (9)	0.3954 (6)	0.5923 (9)
		$Pr_5(Al_xSi_{1-x})_4$ *tP36-*Zr_5Si_4	58.0, 4.0, 38.0	0.7890 (8)		1.4948 (9)
25	54.0, 3.0, 43.0	$Pr(Al_xSi_{1-x})$ *oP8-FeB*	51.0, 1.5, 47.5,	0.8229 (4)	0.3944 (2)	0.5912 (3)
		$Pr_5(Al_xSi_{1-x})_4$ *tP36-*Zr_5Si_4	58.5, 2.5, 38.0	0.7905 (4)		1.4925 (9)
26	53.0, 8.5, 38.5	$Pr_5(Al_xSi_{1-x})_3$ *tI32-*Cr_5B_3	61.0, 4.5, 34.5	0.7803 (2)		1.3656 (6)
		$Pr_5(Al_xSi_{1-x})_4$ *tP36-*Zr_5Si_4	55.0, 3.0, 42.5	0.7919 (9)		1.4907 (9)
		$Pr(Al_xSi_{1-x})$ *oP8-FeB*	50.0, 10.0, 40.0	0.8247 (6)	0.3949 (6)	0.5922 (5)
27	56.5, 13.0, 30.5	$Pr(Al_xSi_{1-x})$ *oP8-FeB*	52.0, 11.5, 36.5	0.8252 (2)	0.3938 (4)	0.5929 (9)
		τ_6 *oS8-CrB*	52.5, 17.5, 30.0	0.4467 (5)	1.1272 (2)	0.4073 (8)
		$Pr_5(Al_xSi_{1-x})_3$ *tI32-*Cr_5B_3	62.0, 6.5, 32.5	0.7817 (7)		1.3692 (2)
28	55.0, 27.0, 18.0	$Pr_5(Al_xSi_{1-x})_3$ *tI32-*Cr_5B_3	61.5, 10.0, 28.5	0.7832 (3)		1.3707 (9)
		τ_6 *oS8-CrB*	53.0, 22.5, 24.5	0.4465 (3)	1.1257 (9)	0.4087 (5)
		PrAl *oP16-ErAl*	53.0, 45.0, 2.0	0.5954 (4)	1.1775 (8)	0.5743 (3)
29	56.0, 40.0, 4.0	Pr_2Al *oP16-*Co_2Si	69.5, 30.5, 0.0	0.6764 (9)	0.5266 (6)	0.9653 (9)
		$Pr_5(Al_xSi_{1-x})_3$ *tI32-*Cr_5B_3	62.0, 21.0, 17. 0	0.7820 (5)		1.3697 (9)
		$Pr(Al_xSi_{1-x})$ *oP8-FeB*	54.0, 46.0, 0.0	0.5967 (5)	1.1741 (9)	0.5743 (8)
30	62.5, 27.0, 10.5	Pr_2Al *oP16-*Co_2Si	68.5, 31.0, 0.5	0.6768 (4)	0.5228 (3)	0.9839 (9)
		$Pr_5(Al_xSi_{1-x})_3$ *tI32-*Cr_5B_3	61.5, 15.0, 22.0	0.7808 (6)		1.3633 (3)
		$Pr(Al_xSi_{1-x})$ *oP8-FeB*	53.5, 46.5, 0.0	0.5959 (8)	1.1744 (8)	0.5740 (9)
31	73.5, 12.5, 14.5	(αPr) *hP4-*αLa	96.5, 3.0, 0.5	0.3658 (4)	0.3658 (4)	1.1831 (7)
		βPr_3Al *cP4-*$AuCu_3$	75.5, 23.5, 1.0	0.4931 (2)		
		$Pr_5(Al_xSi_{1-x})_3$ *tI32-*Cr_5B_3	62.5, 6.0, 31.5	0.7807 (1)		1.3740 (3)

system was assessed by Okamoto [13], and in this system, five intermetallic compounds have been recognized: Pr_5Si_3 (tI32-Cr_5B_3 type), Pr_5Si_4 (tP36-Zr_5Si_4 type), PrSi (oP8-FeB type), $PrSi_{1.33}$ (oC20-Ho_3Si_4 type), $PrSi_2$ (tI12-Th_2Si type, $T > 653$ K and oI12-$GdSi_2$ type $T < 653$ K). The Pr–Al phase diagram has been recently assessed by Jin et al. [14] confirming the following intermediate phases: Pr_3Al (hP8-Ni_3Sn type $T < 330°$, cP4-$AuCu_3$ type $T > 330$ °C), Pr_2Al (oP12-Co_2Si type), PrAl (oP16-AlEr type $T < 700$ °C K, oC16-AlCe type $T > 700$ °C), $PrAl_2$ (cF24-$MgCu_2$ type), $PrAl_3$ (hP8-Ni_3Sn type) and Pr_3Al_{11} (oI28-La_3Al_{11} type $T < 651$ °C, tI10-Al_3Ba type $T > 651$ °C).

Pr–Al–Si ternary system

Nakonechna et al. [15] investigated the Al richest corner of the Pr–Al–Si system at 400 °C. In this system, the following phases are known: $PrAl_2Si_2$ (hP5-$CaAl_2Si_2$ type) [15], $Pr_3Al_4Si_6$ (hP13-$Ce_3Al_4Si_6$ type) [15], $PrAlSi_2$ (hP8-$CeaAlSi_2$ type) [16] Pr_2Al_3Si (hP3-AlB_2 type) [15],

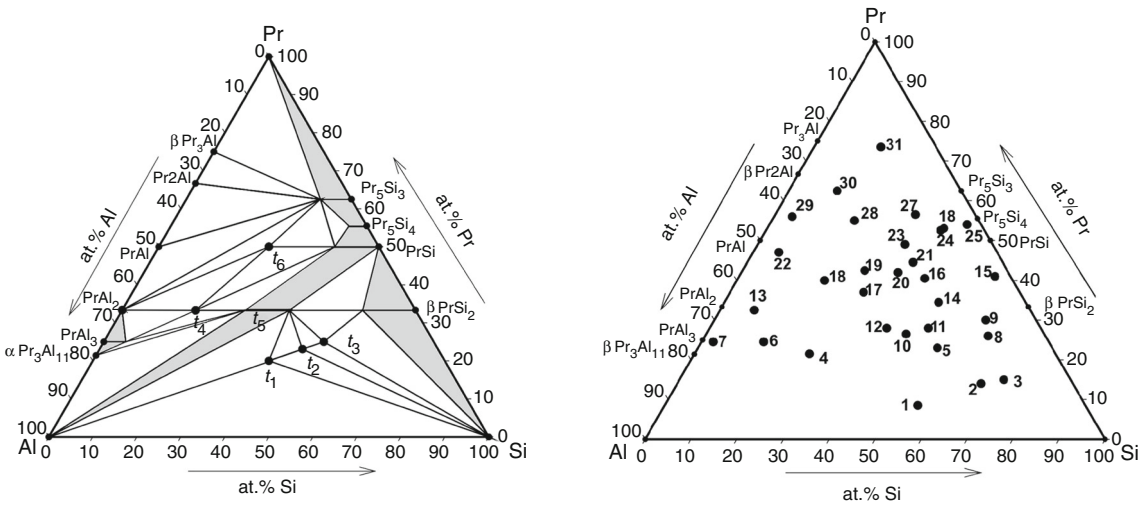

Fig. 1 Pr–Al–Si system. **a** The isothermal section at 500 °C of the Pr–Al–Si system. **b** Gross composition of the analysed alloys. The results of the characterization of the coded samples are shown in Table 1

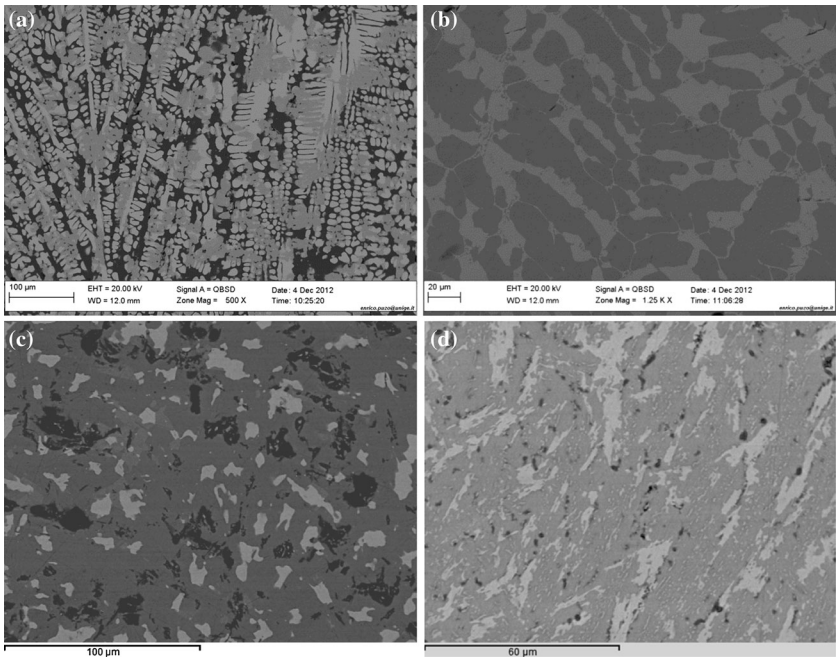

Fig. 2 Back-scattered electron (BSE) images of selected samples annealed at 500 °C (see Table 1). **a** Sample n. 3: τ_2 (*white*), τ_3 (*light grey*) and (Si) (*black*). **b** Sample n. 15: two-phase sample $PrAl_xSi_{1-x}$ (*white crystals*) and $\beta Pr(Al_xSi_{1-x})_2$ (*black*). **c** Sample n. 10: τ_2 (*white*), τ_3 (*grey*) and τ_5 (*black*). **d** Sample n. 27: τ_6 (*white*), $Pr_5(Al_xSi_{1-x})_3$ (*grey*) and $Pr(Al_xSi_{1-x})$ (*black*)

$PrAl_{(1-x)}Si_{(1+x)}$ (tI12-$\alpha ThSi_2$ type) [17], Pr_2AlSi (tI12-$\alpha ThSi_2$ type) [18].

Experimental

Ingots of high-purity metal Pr (99.9 mass% nominal purity), Si (99.999 mass% nominal purity) and Al (99.99 mass% nominal purity) were used to synthesize the alloys (1–2 g each). All the metals were provided by Newmet Koch, Waltham Abbey, England. The samples were prepared by arc melting, under argon atmosphere, stoichiometric amounts of the elements. The mass losses of the alloys during melting were less than 0.2 mass%. The samples, placed in alumina crucibles sealed under vacuum in quartz tubes, were then annealed at 500 °C for 3 weeks and subsequently quenched in cold water. A number of alloys were subjected to DTA by using the Netzsch model

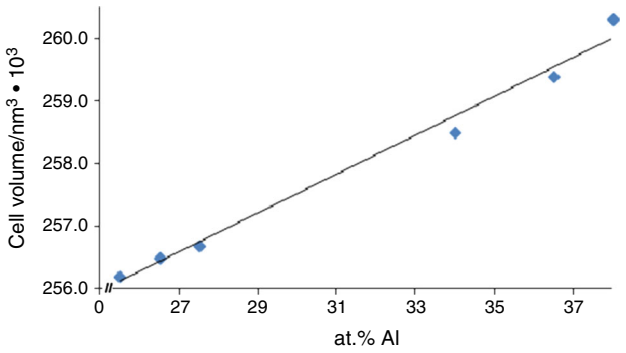

Fig. 3 Unit cell volume of the τ_5 intermediate phase versus the Al content (at.%)

404S apparatus (Selb, Germany), and the measurements were taken, both on heating and on cooling, at different rates (5–10 K min^{-1}). The thermocouples were calibrated by using high-purity elements such as Al, Ag, Au. More details on the operating conditions are reported in [9].

Light optical microscopy (LOM), scanning electron microscopy and electron probe microanalysis based on energy-dispersive X-ray spectroscopy (EDXS) were used to characterize the samples, investigating the microstructure and determining the phase composition. For microscopic observation and metallographic analysis, the specimens were prepared by using SiC papers and diamond pastes down to 3 µm grain size. For the quantitative analysis, an acceleration voltage of 20 kV was applied for 50 s, and a cobalt standard was used for calibration. The software packaging Inca Energy (Oxford Instruments, Analytical Ltd, Bucks, UK) was employed to process X-ray spectra. In order to determine crystal structures and calculate lattice parameters, X-ray diffraction (XRPD) analysis was performed on pulverized samples by using a vertical diffractometer X'Pert MPD (Philips, Amelo, the Netherlands). The indexing of the obtained diffraction data was performed by comparison with the literature or calculated data (the program Powder Cell [19]), and the lattice parameters of the phases were calculated using the program LATCON [20].

Results and discussion

The data obtained in the investigation by SEM/EDXS and X-ray powder diffraction of the different alloys are reported in Table 1. Basing on the experimental results achieved, the Pr–Al–Si isothermal section at 500 °C is drawn and reported in Fig. 1a. Figure 1b shows the compositions of the alloys investigated. Photomicrographs of selected samples are shown in Fig. 2a–d.

Isothermal section

The following binary intermetallic compounds pertaining to the Pr–Al–Si system were confirmed at 500 °C: Pr_5Si_3 (tI32-Cr_5B_3), Pr_5Si_4 (tP36-Zr_5Si_4), PrSi (oP8-FeB), $PrSi_2$ (tI12-Th_2Si), Pr_3Al (cP4-$AuCu_3$), Pr_2Al (oP12-Co_2Si), PrAl (oP16-AlEr), $PrAl_2$ (cF24), $PrAl_3$ (hP8-Ni_3Sn) and Pr_3Al_{11} (oI28-La_3Al_{11}). Five ternary intermetallic compounds, already reported in literature, were identified at 500 °C: τ_1-$PrAl_2Si_2$ (hP5-$CaAl_2Si_2$ type), τ_2-$Pr_3Al_4Si_6$ (hP13-$Ce_3Al_4Si_6$ type), τ_3-PrAlSi2 (hP8-$CeaAlSi_2$ type), τ_4-Pr_2Al_3Si (hP3-AlB_2 type), τ_5-$PrAl_{(1-x)}Si_{(1+x)}$ (tI12-$\alpha ThSi_2$ type) and τ_6-Pr_2AlSi (oS8-CrB).

The τ_5 compound shows an homogeneity range, at a constant Pr content (33.3 at.%), extending towards both the

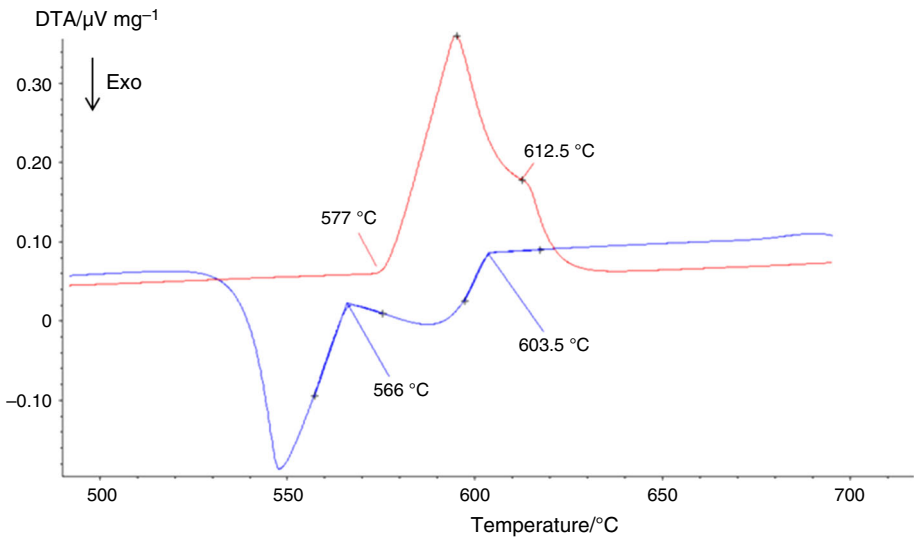

Fig. 4 DTA cooling curve of the alloy at Pr 1 at.%, Al 91 at.%, Si 8 at.% composition

Al richest and Si richest compositions with respect to the stoichiometric formula PrAlSi. The substitution with aluminium for silicon in the τ_5 compound was suggested by Bobev et al. [17], but at 500 °C also the substitution with silicon for aluminium occurs. The compound exists in a range from 28 to 38 at.% aluminium. Figure 3 shows the trend of the τ_5 phase cell volume versus the Al content.

On the basis of the similar atomic radii of the two Al and Si atoms, some solid solutions extend from the binary edges into the ternary field. From the binary Pr–Al system, only one intermetallic compound originates a ternary solid solution: $Pr(Al_{1-x}Si_x)_3$ ($0 \leq x \leq 0.05$, hP16-Ni_3Ti). From the Pr–Si system, five ternary solid solutions form: $Pr(Al_xSi_{1-x})_2$ ($0 \leq x \leq 0.35$, tI2-$ThSi_2$), $Pr_3(Al_xSi_{1-x})_5$ ($0 \leq x \leq 0.15$, hP3-AlB_2), $Pr(Al_xSi_{1-x})$ ($0 \leq x \leq 0.2$, oP8-FeB), $Pr_5(Al_xSi_{4-x})$ ($0 \leq x \leq 0.07$, oP36-Pr_5Ge_4) and $Pr_5(Al_xSi_{3-x})$ ($0 \leq x \leq 0.1$, hP16-Mn_5Si_3). The homogeneity ranges were determined by SEM/EDXS analysis, and the Al/Si mutual substitutions were confirmed by the variation of the lattice parameters of the phases, by moving from the binary into the ternary system. Solid solutions based on binary phases extending less that 2 % in the ternary field were not taken into account.

By comparing the four isothermal sections of the systems Nd–Al–Si [9], Pr–Al–Si, Dy–Al–Si [10] and Sm–Al–Si [11] at 500 °C, moving from the lighter to the heavier lanthanide, it can be observed that there is a regular trend of the number and stoichiometry of the phases. A few Pr–Al–Si samples were subjected to DTA. Figure 4 reveals the heating and cooling curves of a sample at composition Pr 1 at.%, Al 91 at.%; the thermal effect at 566 °C corresponds to the ternary eutectic $L \rightleftarrows (\alpha Al) + (\beta Si) + \tau_1$. The lowering of the eutectic temperature, due to the addition of the rare earth, has been confirmed.

Conclusions

The phase relationships in the Pr–Al–Si system at 500 °C has been drawn, by comparing and analysing the experimental results obtained for 31 samples; 23 three-phase fields and 9 two-phase fields have been determined. The regular trend in the chemical and physical properties through the lanthanides series leads the interaction of Pr with Al and Si at 500 °C to be similar with the other *R*–Al–Si (*R* = light rare earth) systems, especially in the Al–Si-rich side of the system. The stoichiometric ternary intermetallic compounds $PrAl_2Si_2$ (τ_1) hP5-$CaAl_2Si_2$, $Pr_3Al_4Si_6$(τ_2) hP13-$Ce_3Al_4Si_6$, $PrAlSi_2$ (τ_3) hP8-CeAlSi2, Pr_2Al_3Si (τ_4) hP3-AlB_2, $PrAl_{(1-x)}Si_{(1+x)}$ (τ_5) tI12-αTh_2Si and Pr_2AlSi (τ_6) oS8-CrB have been confirmed, and the ternary compound $PrAl_{(1-x)}Si_{(1+x)}$ (τ_5) extends in a composition range from 28 to 38 at.% aluminium, at a constant praseodymium content. The phase cell volume increases regularly with the increase in aluminium content. The isothermal sections studied can be fruitfully compared, concerning the alloying behaviour of the rare earths with Al and Si: the elements Nd, Pr and Sm as examples of the behaviour of the light rare earths, while Dy as the heavy lanthanides. All the systems are characterized by intermediate phases with an *R* content up to 60 at.% rare earth. The number of phases decreases on going from the light to the heavy rare earths. Only the RAl_2Si_2 compound forms along the whole lanthanide series. With respect to the other *R*–Al–Si ternary systems, although the literature data are generally lacking, information is available concerning the Al–Si-rich portion of the different systems, likely due to the technological relevance of the alloys lying near the Al–Si eutectic composition. All the known systems show the tie triangle (Al), (Si) and RAl_2Si_2 (hP5-$CaAl_2Si_2$ type), in which is located the ternary eutectic equilibrium $L \rightleftarrows (\alpha Al) + (\beta Si) + RAl_2Si_2$ ($\tau 1$).

References

1. Miller WS, Zhuang L, Bottema J, Wittebrood AJ, De Pret P, Haszler A, Vieregge A. Recent development in aluminium alloys for the automotive industry. Mater Sci Eng, A. 2000;280:37–49.
2. Chen CL, Richter A, Thomson RC. Mechanical properties of intermetallic phases in multi-component Al–Si alloys using nanoindentation. Intermetallics. 2009;17:634–41.
3. Ye HJ. An overview of the development of Al–Si-alloy based material for engine applications. J Mater Eng Perform. 2003;12:288–97.
4. Zhu M, Jian Z, Yao L, Liu C, Yang G, Zhou Y. Effect of mischmetal modification treatment on the microstructure, tensile properties, and fracture behavior of Al–7.0%Si–0.3%Mg foundry aluminum alloys. J Mater Sci. 2011;46:2685–94.
5. Qiu H, Yan H, Hu Z. Effect of samarium (Pr) addition on the microstructures and mechanical properties of Al–7Si–0.7 Mg alloys. J Alloys Compd. 2013;567:77–81.
6. Mazahery A, Shabani MO. Modification mechanism and microstructural characteristics of eutectic Si in casting Al–Si alloys: a review on experimental and numerical studies. J Miner Met Mater Soc. 2014;166(5):726–38.
7. Heusler L, Schneider W. Influence of alloying elements on the thermal analysis results of Al–Si cast alloys. J Light Met. 2002;2:17–26.
8. Nogita K, Yasuda H, Yoshiya M, McDonald SD, Uesugi K, Tacheuchi A, Suzuki Y. The role of trace element segregation in the eutectic modification of hypoeutectic Al–Si alloys. J Alloys Compd. 2010;489:415–20.
9. Cardinale AM, Macciò D, Delfino S, Saccone A. Experimental investigation of the Nd–Al–Si system. J Therm Anal Calorim. 2011;103:103–9.
10. Cardinale AM, Macciò D, Delfino S, Saccone A. Phase equilibria of the Dy–Al–Si system at 500°C. J Therm Anal Calorim. 2012;108:817–23.
11. Cardinale AM, Macciò D, Delfino S, Saccone A. Phase equilibria in the Sm–Al–Si system at 500°C. J Therm Anal Calorim. 2014;116:61–7.

12. Murray JL, McAlister AJ. The Al–Si (aluminum–silicon) system. Bull Alloy Phase Diagr. 1984;5:74–84.
13. Okamoto H. Desk handbook: phase diagrams for binary alloys. Materials Park: ASM Internatinal; 2000.
14. Jin LL, Kang YB, Chartrand P, Fuerst CD. Thermodynamic evaluation and optimization of Al–La, Al–Ce, Al–Pr, Al–Nd and Al–Pr systems using the modified quasichemical model for liquids. CALPHAD Comput Coupling Phase Diagr Thermochem. 2011;35:30–41.
15. Nakonechna N, Lyaskovska N, Romaniv O, Starodub P, Gladyshevskii E. Pr–Al–Si phase diagram (0–0.33 at.fract. Pr) and crystal structure of the compounds. Visn Lviv Univ Ser Khim. 2001;40:61–7.
16. Muts N, Gladyshevskii RE, Gladyshevskii EI. Crystal structures of the compounds $PrAl_2Si_2$, $Pr_3Al_4Si_6$ and $PrAlSi_2$. J Alloys Compd. 2005;402:66–9.
17. Bobev S, Tobash PH, Fritsch V, Thompson JD, Hundley MF, Sarrao JL, Fisk Z. Ternary rare-earth alumo-silicides—single-crystal growth from Al flux, structural and physical properties. J Solid State Chem. 2005;178:2091–103.
18. Lyaskovska N, Romaniv O, Semus'o N, Gladyshevskii E. Crystal structures of the compounds $RAl_{0.5-x}Si_{0.5+x}$ (R = La, Ce, Pr, Nd, Pr, Gd), $R_3Al_4Si_6$ (R = La, Pr), and $RAlSi_2$ (R = Pr, Nd). J Alloys Compd. 2004;367:180–4.
19. Kraus W, Nolze G. Powder cell for windows. Berlin: Federal Institute for Materials Research and Testing; 1999.
20. King G, Schwarzenbach D. Latcon. In: Hall SR, Du Boulay DJ, Olthof-Hazekamp R, editors. Xtal3.7 system. Perth: University of Western Australia; 2000.